STRUCTURE, PHONON VIBRATIONAND ELECTRICALPROPERTIESOFBa^{2+} DOPEDBISMUTH FERRITE

J. Ahmad[*1], S.A. Ali[1], S.H. Bukhari[2], H. Abbas[1], J.A. Khan[1], U. Nissar[1], T. Sultan[3] and A. Latif[3]

[1]Department of Physics, Bahauddin Zakariya University 60800, Multan Pakistan
[2]Department of Physics, GC University Faisalabad, Sub-Campus, Layyah 31200, Pakistan
[3]Department of Civil Engineering, Bahauddin Zakariya University, Multan 60800, Pakistan
[*]Corresponding Author: javedahmad@bzu.edu.pk, dr.j.ahmad@gmail.com

ABSTRACT: Multiferroic $Bi_{1-x}Ba_xFeO_3$ (BBFO) (x = 0.0, 0.1, 0.2, 0.25, 0.3) nanoparticles were successfully synthesized utilizing sol–gel process. The structure of the prepared samples was characterized by employing x-ray diffraction technique. The results confirmed the transformation of crystal structure from rhombohedral to tetragonal at $x \geq 0.25$. Infrared (IR) reflectivity spectra measured at ambient temperature in the frequency range 10-7500 cm^{-1}. The resonant frequency, oscillator strength and the damping factor of all modes were computed by fitting the IR reflectivity spectra to the classical Lorentz oscillator model. From the temperature dependent electrical resistivity, Ba^{2+} doped BFO exhibited metallic behavior at low temperature, which transform to semiconducting behavior on increasing the temperature. The temperature of this metal to semiconductor (MS) transition depends on doping concentration of Barium.

Keywords: multiferroic materials, sol-gel method, ms transition, IR reflectance spectroscopy.

(Received 03.02.2021 Accepted 28.03.2021)

INTRODUCTION

Multifunctional materials are the materials that perform more than one function in a framework due to their particular properties. There has been a restoration of interest for creating multiferroic having simultaneous ferroelectric polarization and magnetic ordering in a same phase (Schmid, 1994; Van Aken, Rivera, Schmid, & Fiebig, 2007). The interplay between charge and magnetism created great interest in the multiferroic, which exhibit at least two ferroic order parameters simultaneously in a single phase (Fiebig, 2005)(Cheong & Mostovoy, 2007). These materials provide great opportunity to manufacture multifunctional devices. Among multiferroic, Bismuth ferrite BFO has fascinating properties for applications in many field. BFO belongs to ABO_3 type of compounds, presence of magneto electric coupling near room temperature (RT) makes BFO a potential nominee for designing novel electronic devices such as; multi-stage memories, magnetically storage applications, actuators, transducers, sensors and emerging spintronic devices (Smolenskiĭ & Chupis, 1982). It belongs to the rhombohedraly contort perovskite formation with space group R3c and has spiral- cycloid magnetic structure (Lobo, Moreira, Lebeugle, & Colson, 2007). It has high ferroelectric (T_C) and antiferromagnetic (T_N) transition temperatures ~1100 K and ~640 K, respectively. The ferromagnetic coupling among Fe magnetic moments within the (111) plane and antiferromagnetic interaction between adjacent planes is the manifestation of G-type antiferromagnetic ordering. If the magnetic moments were align perpendicular to the [111] direction, than reduced symmetry allow a canting of the antiferromagnetic sub lattices, resulting in weak ferromagnetism. But contrary to this, the magnetoelectric (ME) effect is limited due to the existence of G-type antiferromagnetic ordering (Khomchenko, Kopcewicz, *et al*., 2008). Applications of BFO have been restricted due to formation of secondary/impurity phases during synthesis process, loss in strength of magnetic coupling, and leakage current and so forth. The replacement of A-site cations by alkaline earth metal (Ba, Ca, and Sr) is a promising way for improving the ferromagnetic property. The spin modulation can be reduced by substituting a suitable divalent cations to attain spontaneous magnetization and also to induce oxygen vacancies (Sosnowska, Neumaier, & Steichele, 1982). The magnetic moment of divalent alkaline earth metals is comparable to that of rare earth substituted BFO (Khomchenko, Kiselev, *et al*., 2008). It has been reported by many researchers that small particles incorporation enhanced the magnetization of BFO and is attributed to the magnetization induced by surface effects.

In this work we adopted Sol–gel processing. It is a delicate chemical method to obtain operational materials at low temperature. This method is exceptionally promising to acquire impurity free advanced nano-materials and to orient the materials properties for specific applications. It also provides fine crystallite size, better multiferroic properties, high purity, greater homogeneity, less cost and simpler equipment as compared to the traditional method of fusing oxides. In

this process we use acetic acid as a solvent to dissolve the respective nitrates.

MATERIALS AND METHODS

BBFO samples with x = 0.0, 0.1, 0.2, 0.25, 0.3 were prepared using sol-gel auto combustion method. The stoichiometric amount of Bismuth nitrate $Bi_5O(OH)_9(NO_3)_4$, Iron (III) nitrate nano-hydrate $Fe(NO_3)_3.9H_2O$ and barium nitrate $Ba(NO_3)_2$ were separately dissolved in acetic acid and continuously stirred until the nitrates dissolved completely. Ethylene alcohol was added in each solution under constant stirring. The color of resultant product was blackish red. The molarity of the final product was adjusted between 0.1 to 0.2 mol. by incorporating proper amount of acetic acid and ethylene alcohol. The solution was heated at about 70 °C to convert it into the gel. The gel was ignited to obtain porous powder by heating at 100 °C for 1 hour and then ground in a mortar and pestle. After grinding powders were sintered in an electric furnace, Nabertherm GNBH, Lilienthal/Bremen Germany, with a uniform increasing temperature variation of 10°C/min until reached at 700 °C and then maintained at this temperature for 1 hour and then quenched to room temperature in air.

Characterizations: PANalytical X'PERT-PRO X-ray diffractometer adjusted at 40 kV and 30 mA, were utilize to examine the crystal structure of the prepared series. The radiation used was Cu Kα (λ= 1.540598 Å) having no monochromator and the data was collected in the range of (2θ) from 20° to 80° with a step of 0.025° and 2400 total scan. The room temperature IR reflectivity spectra of samples were recorded in the frequency range of 10-7500 cm^{-1}, using a BRUKER, Vertex 80V FTIR Spectrometer. To study the conduction mechanism Keithley 2400 source meter is used in the temperature range 290-400 K with pressure contacts. To measure dielectric properties LCR Meter-8101GW Instek covering frequency from (20 Hz - 1 MHz) is used.

RESULTS AND DISCUSSION

Figure1 shows the XRD graph for BBFO with x = 0.0, 0.1, 0.2, 0.25, 0.3 at RT. The main phase is BBFO along with a small amount of secondary phase $BaFe_2O_4$, which reduces as the Ba^{2+} concentration is increased. This impurity phase is due to the uncontrolled auto-ignited process during synthesis.

The indexing of all the diffraction peaks were performed with combination of rhombohedral-tetragonal structure having its space group R3c as the Ba concentration increases, intensity of reflected peaks decrease but the full width half maxima (FWHM) increases which shows the formation of refined crystallite. All diffraction Peaks were indexed by comparing their "d" values with standard pattern of lines according to the JCPDS card no. 71-2494. The obtained crystallite size (D) for each sample was calculated from XRD data by employing Scherer equation.

$$D = K\lambda / (\beta\cos\theta) \quad (1)$$

$$d_{X\text{-}ray} = Z.M / N_A V_{cell} \quad (2)$$

$$V_{cell} = abc \sin\gamma \quad (3)$$

where 'K' is the constant having value of 0.9, 'λ' the x-ray wavelength 'β' is the FWHM and 'θ' is the diffraction angle. X-ray density can be measured by formula, Where, Z = number of formula unit (f.u.), M = molecular weight, N_A = Avogadro's number, V_{cell} = unit cell volume. The structural parameters were calculated by using XRD data. Mathematically, assuming hexagonal system for samples, unit cell volume is;

For rhombohedral and tetragonal system, $a = b \neq c$, $\gamma = 120^0$ and $\gamma = 90^0$, respectively.

Bulk density and porosity was calculated as

$$d_{bulk} = m / V \quad (4)$$

$$P = (1\text{-}d_B/d_x).100 \quad (5)$$

where 'm' = mass in grams, volume = $\pi r^2 L$. It can be seen from the Figure1 that for the samples x = 2.5 and x = 3; the highest intensity double peak (2θ ~ 32°) is merged into single peak, similar merging of peaks is observed at ~51° and ~56°. It may be due to the result of transformation of crystal structure from rhombohedral to tetragonal for x = 0.25 and above, same type of trend was also reported by Chou Yang *et. al*(Yang *et al*., 2010).

The obtained structural parameters as computed are given in the table 1. The crystallite size (D) of all the samples were calculated and found between 35 to 70 nm. The crystallite size and unit cell volume increase as the Ba^{+2} concentration increases up to x = 0.20 is attributed to the fact that the ionic size of Ba^{2+} (1.36 Å) is larger as compared to Bi^{3+}(1.17 Å) and then decrease abruptly as the system is transforming from a state lower symmetry to the state of higher symmetry. The $d_{X\text{-}ray}$ and d_{bulk} decrease with the increase in Ba^{+2} amount up to x = 0.20 and increase for x = 0.25 & x = 0.30.

The fluctuation among the lattice parameters a, c, bulk density, X-ray density, unit cell volume and porosity at various dopant concentrations are shown in Table 1. It is obvious that porosity gets increased with an increase in the concentration. The rise in porosity is the result of segregation of small vacancies into the lattice when larger cation replaces the smaller one.

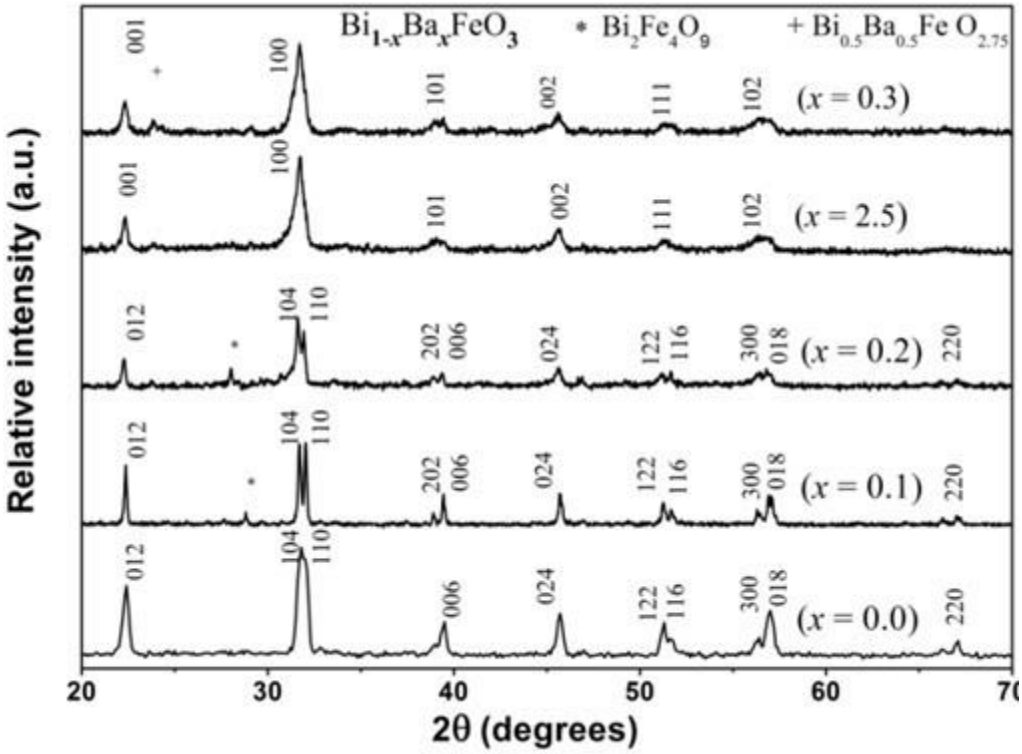

Fig. 1. Combined x-ray diffraction pattern for BBFO with *x* = 0.00, 0.1, 0.2, 0.25 and 0.3.$Bi_{1-x}Ba_xFeO_3$ (*x* = 0.0, 0.10, 0.20, 0.25 and 0.30)

Table 1. Shows crystal structure, crystallite size, lattice parameters, unit cell volume, x-ray density, bulk density and porosity of samples

Sr.No.	Samples	Crystalline structure	D (nm)	a (Å)	c (Å)	V_{cell} $(Å)^3$	$d_{X\text{-}ray}$ (g/cm^3)	d_b=m/V (g/cm^3)	Porosity (%)
1	$BiFeO_3$	Rhombohedral	43.30	5.62	13.67	250.87	12.42	6.10	51
2	$Bi_{0.9}Ba_{0.10}FeO_3$	Rhombohedral	56.09	5.58	13.89	251.68	12.10	5.67	53
3	$Bi_{0.80}Ba_{0.20}FeO_3$	Rhombohedral	67.87	5.77	13.71	265.58	11.20	3.37	69
4	$Bi_{0.75}Ba_{0.25}FeO_3$	Tetragonal	39.02	2.81	3.97	31.54	93.18	4.60	93
5	$Bi_{0.70}Ba_{0.30}FeO_3$	Tetragonal	37.25	2.80	3.96	31.15	93.20	4.66	95

IR Reflectance Analysis: The reflectivity spectrum of undoped BFO is shown in the inset of Figure 2. Below 1000 cm^{-1}, the spectrum consists of several peaks while it remains almost flat above 1000 cm^{-1}. This structure less spectrum above 1000 cm^{-1} indicates the non-existence of any optical process and thus would not be included in the later discussion. Thus here is emphasized only on the spectrum below 1000 cm^{-1}, which exhibits several peaks. These peaks are associated to optical phonon modes. Figure 2 shows IR reflectivity spectra for all samples for frequency between 10 cm^{-1} and 1000 cm^{-1}. As Ba^{2+} doping increases in BFO, the reflectivity spectrum lifts up and the background contribution below the phonon spectrum increases. At above *x* = 0.25, the background reflectivity contribution becomes significant and also the shape of the spectrum deviates from that of typical semiconductor. It is more clear from the reflectivity spectrum for *x* = 0.3, the sample with maximum doping of the Ba^{+2} in BFO in the present study, that the phonons are almost screened by the background contribution. The background contribution to reflectivity in the mid infrared region is due to free electrons or small polarons (Ahmad & Uwe, 2005). The values of the resonant frequencies, oscillation strength and the damping parameter of the infrared active phonon modes have been determined by fitting the reflectivity spectra (Figure 3) using the classical LO model, in which the dielectric constant is defined as

$$\varepsilon(\omega) = \varepsilon_{\infty} + \sum_{j} \frac{\omega_{TOj}^2 S_j}{\omega_{TOj}^2 - \omega^2 - i\omega\gamma_j}, \quad (6)$$

Where, ε_∞ is the permittivity due to high frequency electronic excitations, ω_{TOj} is the transverse optical (TO) phonon frequency, S_j is the oscillator strength and γ_j is the damping factor of the jth optical phonon. The near normal incidence reflectivity is obtained from the Fresnel formula,

$$R = \left| (\sqrt{\varepsilon} - 1) \Big/ (\sqrt{\varepsilon} + 1) \right|^2 \quad (7)$$

On increasing the *x*, the resonant frequency ω_{TO} of all modes except the highest frequency mode either remains unchanged or increases slightly (see Table 2). The highest frequency mode surely shifts towards low frequency on increasing the Ba^{2+} doping; ω_{TO} = 560 cm^{-1} at *x* = 0 reduces to ω_{TO}= 548 cm^{-1} at *x* = 0.2 and thus behaves as a soft mode. This high frequency mode arises due to the stretching of oxygen atoms in the FeO_6 octahedra and thus results in a change of Fe-O bond length. The phonon softening of the highest frequency mode indicates some sort of coupling with the electronic excitations.

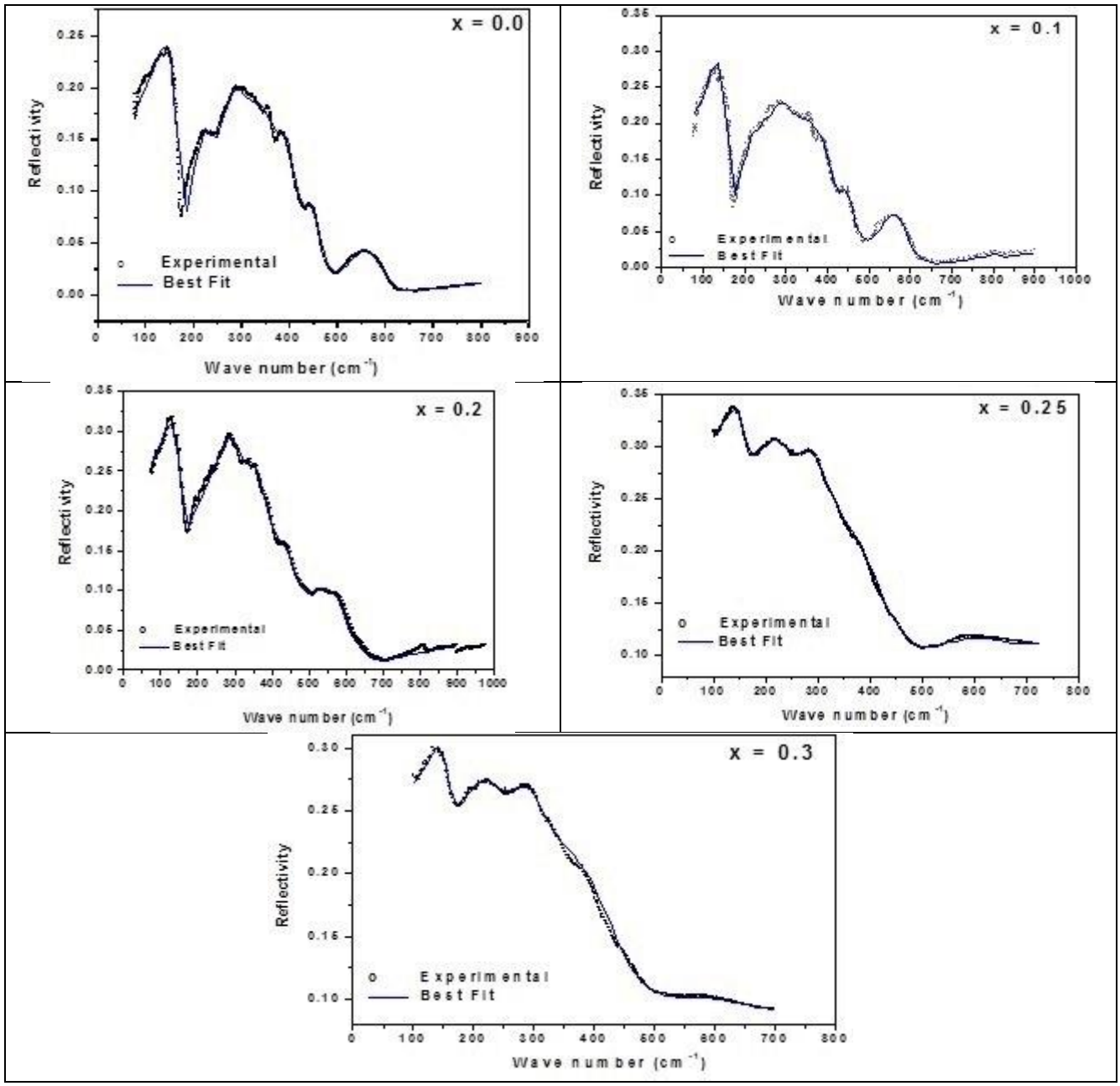

Fig. 2. Comparison of all FT-IR Reflectivity spectrums for $Bi_{1-x}Ba_xFeO_3$.

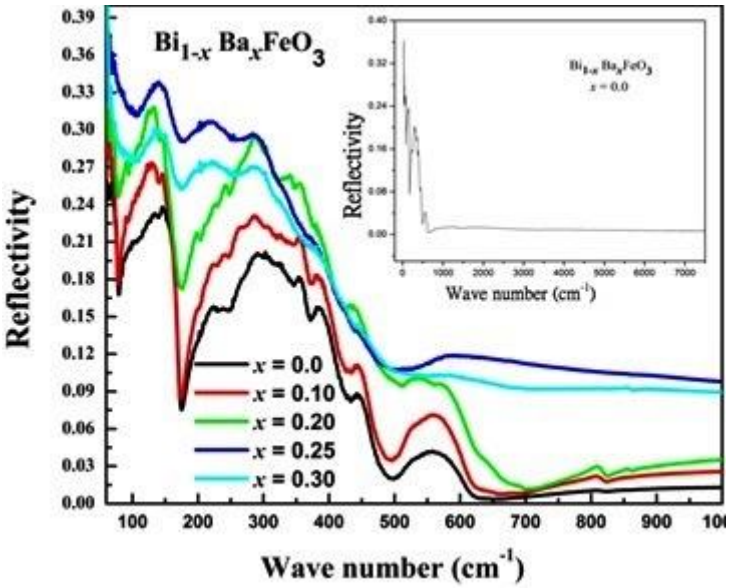

Fig. 3.Lorentz fit IR reflectivity spectra for $Bi_{1-x}Ba_xFeO_3$.

Table 2. Fit parameters used to best fit the data using Lorentz oscillator model for $Bi_{1-x}Ba_xFeO_3$.

	***x* = 0.0**	***x* = 0.10**	***x* = 0.20**	***x* = 0.25**	***x* = 0.30**
ω_{TO1}	145	138	135	152	152
ω_{TO2}	228	223	----------	227	229
ω_{TO3}	286	285	289	294	295
ω_{TO4}	340	350	349	----------	----------
ω_{TO5}	389	383	----------	381	385
ω_{TO6}	442	444	435	----------	----------
ω_{TO7}	560	556	548	----------	----------
S_1	1.53	1.97	2.26	1.40	0.89
S_2	0.18	0.02	----------	1.39	0.98
S_3	0.69	1.17	2.46	1.17	0.88
S_4	0.57	0.61	0.49	----------	----------
S_5	0.11	0.15	----------	1.58	1.64
S_6	0.06	0.04	0.21	----------	----------
S_7	0.14	0.17	0.32	----------	----------
γ_1	45.00	45.33	50.00	48.36	40.79
γ_2	32.89	9.01	----------	86.17	85.54
γ_3	72.94	95.96	130.00	93.66	90.70
γ_4	96.41	121.71	102.17	----------	----------
γ_5	52.02	105.58	----------	200.00	200.01
γ_6	45.03	31.26	94.44	----------	----------
γ_7	92.80	84.11	129.99	----------	----------
ε_∞	2.024	2.22	2.65	5.16	4.50

Electrical Resistivity: Figure 4 shows the DC resistivity graph for all samples with respect to temperature. The general trend for log resistivityvs. temperature of all the samples is almost similar. Each resistivity curve may be divided into two regions; metallic and semiconducting regions, in lower range of temperature they show metallic behavior whereas semiconducting behavior is dominated in the higher range, It is clear that below a certain Transition temperature T_{MS} resistivity increases with temperature, but above the T_{MS}it decreases as temperature increases. Similar type of trend was reported by A.Azam*et. al.*(Azam, Jawad, Ahmed, Chaman, & Naqvi,

2011) for Al^{+3}dope BFO samples. In the metallic region the resistivity increases due to three types of scattering mechanisms, electron-electron (e-e), electron-phonon (e-p) and electron-magnon (e-m) contribution. These scatterings are dominated by the thermal activation process at higher temperature. Also it can be seen from

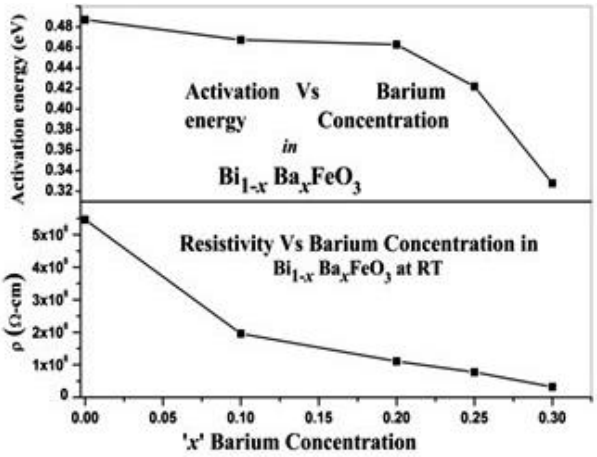

Fig. 4. The resistivity change and activation energy as a function of Barium concentration $Bi_{1-x}Ba_xFeO_3$

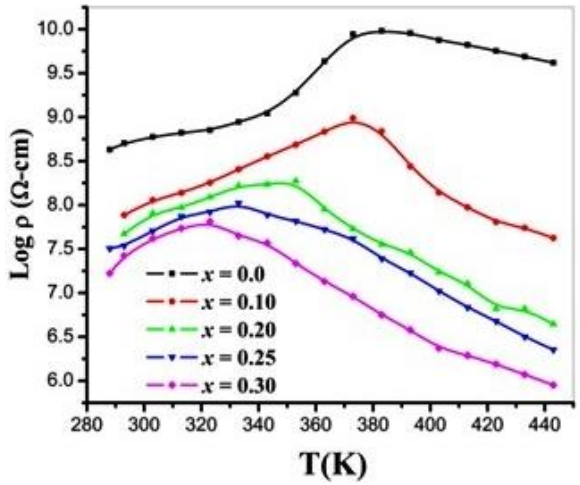

Fig. 5. DC resistivity variations with temperature for $Bi_{1-x}Ba_xFeO_3$

Table 3 that the metal to semiconductor transition temperature (T_{MS}) shifts towards the lower temperature as Ba^{+2} concentration increases. This variation may be due to the fact that Ionization energy of Ba (502.9 kJ/mol) is less than that of Bi (703kJ/mol). As the Ba^{2+} concentration is increases resistivity decreases for all temperatures and consistent with the IR reflectivity results. Resistivity in metallic region can be explained with the help of model $\rho(T) = \rho_o+\beta T^2+\gamma T$,in this model ρ_o is residual resistivity at T = 0, β and γ are electron-electron (e-e) scattering and electron-phonon (e-p) scattering coefficients, respectively. Semiconducting due to the fact that as electron becomes thermally excited it jumps to the conduction band and decreases as the Ba^{2+} concentration increases as the doping element is metallic in nature. Figure 5 **s**hows the Arrhenius plots .The slop is obtained by taking linear fit of natural log of resistivity (ρ) vs. 1000/T. Slope of the curve decreases as the Ba^{+2} concentration increases due to the fact that doping element is chosen from the 2nd group elements in periodic table. Therefore, the value of resistivity (ρ) also decreases from 5.46E8 Ω-cm to 0.32E8 Ω-cm as the Ba^{2+} concentration increases see table 3.

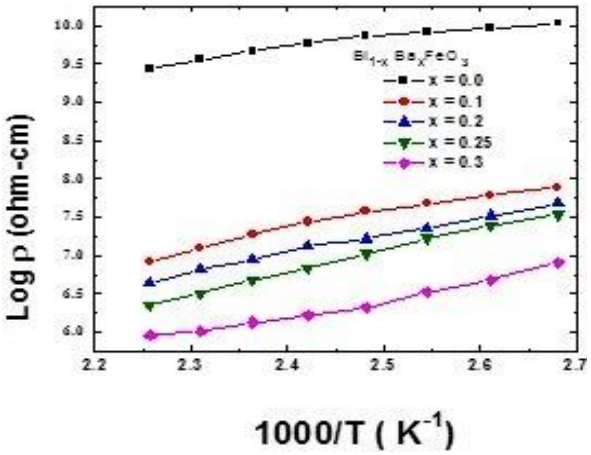

Figure 6. Combined graph of the log of resistivity as a function of 1000/T (K^{-1}) for $Bi_{1-x}Ba_xFeO_3$

Table 3. Shows the transition temperature T_{MS} and value of resistivity at room temperature

Concentration *X*	Transition Temperature T_{MS} (Kelvin)	Room Temperature Resistivity (Ω-Cm)
0.00	383	5.46E8
0.10	353	1.96E8
0.20	343	1.11E8
0.25	303	0.77E8
0.30	293	0.32E8

Conclusion: Ba^{2+} substituted BFO multiferroics were successfully prepared by sol-gel method. Reflectivity spectrum of BFO is like that of a typical semiconductor, which changes to that of metal on increasing Ba^{2+} concentrations. On increasing Ba^{2+} concentrations the highest frequency phonon shifts towards the low frequency mode which dictates some sort of coupling with electronic excitation. Electrical resistivity dictates metal to semiconductor transition of Ba^{2+} substituted BFO with the increase in temperature.

Acknowledgement: The financial support of the HEC, Pakistan through its NRPU No. 9301/Punjab/NRPU/R&D/HEC/2017 is greatly acknowledged.

REFERENCES

Ahmad, J., & Uwe, H. (2005). Small-polaron excitations in Ba 1− x K x Bi O 3 studied by optical reflectivity measurements. *Physical Review B, 72*(12), 125103.

Azam, A., Jawad, A., Ahmed, A. S., Chaman, M., & Naqvi, A. H. (2011). Structural, optical and transport properties of Al3+ doped BiFeO3 nanopowder synthesized by solution combustion method. *Journal of Alloys and Compounds, 509*(6), 2909-2913.

Cheong, S.-W., & Mostovoy, M. (2007). Multiferroics: a magnetic twist for ferroelectricity. *Nature materials, 6*(1), 13-20.

Fiebig, M. (2005). Revival of the magnetoelectric effect. *Journal of physics D: applied physics, 38*(8), R123.

Khomchenko, V. A., Kiselev, D. A., Vieira, J. M., Jian, L., Kholkin, A. L., Lopes, A. M. L., . . . Maglione, M. (2008). Effect of diamagnetic Ca, Sr, Pb, and Ba substitution on the crystal structure and multiferroic properties of the BiFeO 3 perovskite. *Journal of applied physics, 103*(2), 024105.

Khomchenko, V. A., Kopcewicz, M., Lopes, A. M. L., Pogorelov, Y. G., Araujo, J. P., Vieira, J. M., & Kholkin, A. L. (2008). Intrinsic nature of the magnetization enhancement in heterovalently doped Bi1− xAxFeO3 (A= Ca, Sr, Pb, Ba) multiferroics. *Journal of physics D: applied physics, 41*(10), 102003.

Lobo, R., Moreira, R. L., Lebeugle, D., & Colson, D. (2007). Infrared phonon dynamics of a multiferroic Bi Fe O 3 single crystal. *Physical Review B, 76*(17), 172105.

Schmid, H. (1994). H. Schmid, Ferroelectrics 162, 317 (1994). *Ferroelectrics, 162*, 317.

Smolenskiĭ, G. A., & Chupis, I. E. (1982). Ferroelectromagnets. *Soviet Physics Uspekhi, 25*(7), 475.

Sosnowska, I., Neumaier, T. P., & Steichele, E. (1982). Spiral magnetic ordering in bismuth ferrite. *Journal of Physics C: Solid State Physics, 15*(23), 4835.

Van Aken, B. B., Rivera, J.-P., Schmid, H., & Fiebig, M. (2007). Observation of ferrotoroidic domains. *Nature, 449*(7163), 702.

Yang, C., Jiang, J.-S., Qian, F.-Z., Jiang, D.-M., Wang, C.-M., & Zhang, W.-G. (2010). Effect of Ba doping on magnetic and dielectric properties of nanocrystalline BiFeO3 at room temperature. *Journal of alloys and compounds, 507*(1), 29-32.